

Identification of an Arbitrary Shape Obstacle of Scattering Problem Using Near Field Data

Tomasz Rymarczyk^{1,2*}, Jan Sikora^{1,2}, Monika Kulisz³, Grzegorz Kłosowski³

¹ Research & Development Centre Netrix S.A., ul. Związkowa 26, 20-148 Lublin, Poland

² Faculty of Transport and Informatics, WSEI University, ul. Projektowa 4, 20-209 Lublin, Poland

³ Faculty of Management, Lublin University of Technology, ul. Nadbystrzycka 38 D, 20-618 Lublin, Poland

* Corresponding author's e-mail: tomasz@rymarczyk.com

ABSTRACT

This paper delves into a significant area of research, exploring the application of the standard boundary element method (BEM) to analyze inverse acoustic frequency scattering problems in 2D space using a rigid corrugated circular object. The inverse problem is reformulated as an optimization problem, with the boundary of the scatterer parametrized to reduce the number of optimization variables. The influence of these parameters on imaging results based on near-field data is examined. The analysis uses a flat wave illuminating the object along the positive x-axis direction. The study evaluates the accuracy of the solution across various parameters defining the boundary of the analyzed object. The findings, which significantly contribute to advancements in computational methods, non-destructive testing, and the understanding of functional properties of materials and structures, offer valuable insights into numerical techniques and their practical engineering applications.

Keywords: boundary element method, near field data, arbitrary shape obstacle, inverse scattering problem.

INTRODUCTION

Acoustic scattering problems are pivotal in various engineering disciplines, and this research bridges the gap between them, including mechanical engineering, material science, and biomedical engineering. The accurate modeling and reconstruction of obstacle shapes based on near-field data are not just theoretical exercises, but are essential for practical applications such as non-destructive testing, medical imaging, and material characterization. The BEM has emerged as a powerful computational tool for solving these complex problems, offering flexibility in imposing boundary conditions and modeling external fields.

Acoustic scattering is when an incident acoustic wave interacts with an object and is deflected in different directions. This process is central to applications such as sonar detection, ultrasound imaging, and structural health monitoring [1]. Accurate

modeling of acoustic scattering allows engineers to predict and analyze the behavior of waves as they encounter different materials and geometries.

The boundary element method is particularly advantageous for solving acoustic scattering problems due to its boundary-only discretization, which reduces the dimensionality of the problem by one [2, 3]. This method is highly effective in handling infinite domains and complex boundary conditions, making it suitable for external field modeling and applications where the surrounding medium extends to infinity [4].

In non-destructive testing, BEM facilitates the detection of flaws in materials without causing damage. By analyzing the scattered field data, engineers can reconstruct the shape and size of internal defects, improving structures' safety and reliability. Similarly, in medical imaging, BEM is used to improve the quality of ultrasound images, aiding in the diagnosis and treatment of various medical conditions [5]. Material characterization

is another area where BEM is invaluable. By studying the scattering patterns, researchers can infer the mechanical properties of materials, such as elasticity, density, and acoustic impedance [6]. This information is critical for developing and improving new materials for industrial applications.

Recent advances in computational techniques and hardware have further enhanced the capabilities of BEM. High-performance computing and parallel processing allow large-scale scattering problems to be solved with greater accuracy and efficiency [1]. In addition, the coupling of BEM with other numerical methods, such as the finite element method (FEM), allows for hybrid approaches that exploit the strengths of each method [7]. Furthermore, integrating machine learning algorithms with BEM has opened new avenues for automatic shape reconstruction and real-time monitoring. These advances promise to revolutionize structural health monitoring and adaptive material design. Computational fluid dynamics models have proven effective in optimizing the design and analysis of engineering systems, which can also be applied to improve acoustic scattering simulations [8].

Recent research indicates the significant potential of deep neural networks to increase the accuracy of diagnostic imaging [9, 10], which may have future applications to acoustic scattering problems in medical and industrial engineering. In addition, advanced stochastic modeling techniques [11] can increase the reliability and performance of diagnostic systems by accurately modeling complex temporal dynamics, enabling further improvements in acoustic scattering applications. Recent advancements in wireless communication technologies have significantly enhanced the efficiency and accuracy of data transmission in wearable electronic devices, which can be leveraged in acoustic scattering applications for real-time monitoring and diagnostics [12].

In engineering mechanics, computational methods are critical in advancing our understanding and solving complex problems. BEM, known for its effectiveness in modeling boundary conditions, provides a robust solution for analyzing acoustic scattering problems. This study focuses on the inverse acoustic scattering problem, which involves reconstructing the shape of obstacles based on near-field measurements. Such problems are not only theoretically challenging but also have significant practical implications in engineering diagnostics and imaging. The inverse

acoustic scattering problem is fundamental to various applications, including non-destructive evaluation and medical diagnostics. Solving these problems requires sophisticated algorithms that can accurately reconstruct the shape and properties of the scattering objects from limited and often noisy data [13]. Recent research has proposed innovative methods, such as the hyper-singular source method, to address the uniqueness and stability issues inherent in inverse problems [14].

The development of advanced BEM techniques, such as the extended isogeometric boundary element method (XIBEM), has significantly improved the accuracy and efficiency of solving medium-wave acoustic scattering problems [15]. These advances allow detailed analysis of complex geometries and materials, providing valuable insights for practical applications. The use of machine learning techniques has shown promise in improving the classification and analysis of complex flow regimes, which can be adapted for acoustic scattering problems [16]. Advanced monitoring systems using electrical capacitance tomography can enhance the detection and analysis of structural defects in materials [17].

In addition, innovative approaches such as the coupled hybrid smoothed radial point interpolation method have been introduced to reduce dispersion errors in underwater acoustic scattering problems, thereby improving the accuracy of reconstructed shapes [2]. Integrating these methods with real-time monitoring systems allows dynamic adjustments and improved diagnostic capabilities.

The importance of solving inverse acoustic problems lies in their application to engineering diagnostics, non-destructive testing, and medical imaging. Inverse acoustic problems involve determining the properties or shape of an object based on measured acoustic waves that have interacted with it [18]. This process is critical for identifying defects in materials, locating sources of acoustic emissions, and imaging internal body structures. Additionally, recent developments in the study of fluid dynamics in segmented orifice flows provide insights that can be applied to the analysis of acoustic scattering in various media [19]

Existing methods for solving inverse acoustic problems include techniques such as the BEM, the FEM, and hybrid approaches. However, these methods face limitations such as computational cost, convergence issues, and sensitivity to noise [20]. For example, conventional BEM requires significant computational resources, especially

for large-scale problems, and can struggle with stability and accuracy when dealing with complex geometries and heterogeneous media [15]. Addressing these limitations is an ongoing area of research, with recent advances focusing on improving computational efficiency and robustness to measurement noise [21]. The Boundary Element Method is a versatile and powerful tool for tackling acoustic scattering problems. Its ability to handle complex boundary conditions and infinite domains and its integration with modern computational techniques make it indispensable across various engineering disciplines. The ongoing research and development in this area continue to expand its applications and improve its effectiveness, solidifying its role in addressing contemporary engineering challenges.

RESEARCH NOVELTY

This study considered the inverse problem of scattering when a flat wave incident on an object of arbitrary shape. Based on measurements of the field at the Gamma boundary surrounding the obstacle, a reconstruction of the obstacle boundary will be considered. For this purpose, the BEM [22–24] was applied due to its ease of modeling external fields (Sommerfeld radiation conditions are automatically fulfilled), flexibility of imposing boundary conditions, and ease of modeling the shape of the boundary line. The problem involves reconstructing the scatterer surface based on near-field measured data. The obstacle is assumed to be a small and smooth perturbation of a disk (corrugated circle). The task poses some limitations, which are listed below:

- Only the shape of the obstacle is reconstructed.
- Incoming wave is flat, harmonic, and analyzed in the frequency domain.
- Environment is a homogeneous medium.
- Boundary conditions: A Neumann boundary condition is assumed at the obstacle boundary, but Dirichlet or Robin conditions can also be easily imposed.
- Sommerfeld radiation condition: Satisfied by the scattered field.

Such problems become essential for engineering problems like medical imaging or non-destructive testing. Many authors explore this or similar topics, such as Jeong et al. [25] or Li and Wang in their excellent paper [26]. In their work, the authors reconstruct only the shape of

the obstacle using near-field measurement data. It is worth noting that the method adopted by the authors is an analytical method with Dirichlet boundary conditions, making it applicable only to ‘sound soft’ obstacles. This method represents a unique approach to solving the inverse scattering problem. However, analytical methods do have certain limitations. Based on numerical analysis using the Boundary Element Method, the proposed approach is accessible from the constraints inherent in analytical methods. However, the proposed approach does not have disadvantages (commonly known ones). It offers advantages such as the ease of imposing the boundary conditions, including Sommerfeld radiation conditions, which are invaluable for this case. In this paper, the solution of the inverse problem was brought to the optimization iterative problem [25]. The objective function and inequality constraints imposed on the design variables were determined. The iterative methods require good initial guesses and are computationally expensive, as a sequence of forward problems needs to be solved at each iteration step. However, such disadvantages can be overcome quite easily in this case.

By collecting data in the near-field zone, it is possible to obtain images with subwavelength resolution. This is referred to as near-field imaging [26] and might be useful for emerging applications in modern science and technology like nanotechnology.

THE FORWARD PROBLEM OF ACOUSTIC SCATTERING

The problem is outlined by beginning with the time-harmonic reduction of the wave Equation for the exterior forward problem to the Helmholtz Equation [27–29]:

$$\nabla^2 \psi(\mathbf{p}, t) = \frac{1}{c^2} \frac{\partial^2}{\partial t^2} \psi(\mathbf{p}, t) \quad (1)$$

where: $\psi(\mathbf{p}, t)$ [m²/s] is the scalar time-dependent velocity potential related to the time-dependent particle velocity by relation $\mathbf{v}(\mathbf{p}, t) = \nabla \psi(\mathbf{p}, t)$ [m/s] (\mathbf{p} and t are the spatial and time variables in meters and seconds respectively) and c [m/s] is the propagation velocity.

Transferring from the time domain to the frequency domain the velocity potential ψ can be expressed as follows:

$$\psi(\mathbf{p}, t) = \text{Re}\{\varphi(\mathbf{p})e^{-i\omega t}\} \quad (2)$$

where: $\omega = 2\pi f$ [1/s], $\varphi(p)$ is the velocity potential amplitude and $i = \sqrt{-1}$ is the imaginary unit. The substitution of the above expression into the wave Equation (1) reduces it to the Helmholtz Equation of the form [22, 30]:

$$\nabla^2 \varphi(p) + k^2 \varphi(p) = Q \quad (3)$$

where: $k^2 = \frac{\omega^2}{c^2}$ and is the wavenumber and the wavelength is equal to $\lambda = c/f$, the right-hand side Q stands for the acoustic source. The complex-valued function $\varphi(p)$ possesses the magnitude and phase shift. The particle velocity has the similar form to the velocity potential see Equation 2:

$$v(p, t) = \text{Re}\{\nabla \varphi(p) e^{-i\omega t}\} \quad (4)$$

Often the normal component of the velocity on the boundary $v_n(p)$ is imposed as a Neumann boundary condition:

$$v_n(p) = \nabla \varphi(p) \cdot n_p = \frac{\partial \varphi(p)}{\partial n_p} \quad (5)$$

where: n_p is the unit outward normal to the boundary at point $p[m]$ (see for example Fig. 1).

The sound pressure p at the point p in the acoustic domain is one of the most useful acoustic properties, and it is related to the velocity potential $\varphi(p)$ by relation:

$$p(p) = i\omega\rho\varphi(p) \left[\frac{1 \text{ kg m}^2}{\text{s m}^3} = \frac{\text{kg}}{\text{ms}^2} = \frac{\text{N}}{\text{m}^2} = \text{Pa} \right] \quad (6)$$

In theoretical acoustics [28], it is often desirable to work with the Helmholtz Equation (3) of the velocity potential φ instead of pressure p and/or vector of the particle velocity v . Taking into account the above considerations and making use of Green's second identity, the Helmholtz Equation 3 can be expressed in an equivalent form of a Boundary Integral Equation (BIE) [31,32], i.e.:

$$c(r)\varphi(r) + \int_{\Gamma} \frac{\partial G(|r-r'|)}{\partial n} \varphi(r') d\Gamma = \int_{\Gamma} G(|r-r'|) \frac{\partial \varphi(r')}{\partial n} d\Gamma + \varphi^{inc}(r), r \in \Gamma \quad (7)$$

where: φ^{inc} is the incident wave and the vector n is the unit normal vector outward pointing from the considered domain (Fig. 1), Γ represents the boundary of the domain under consideration.

The sound-hard scatterer is imposed through a homogeneous Neumann boundary condition on the

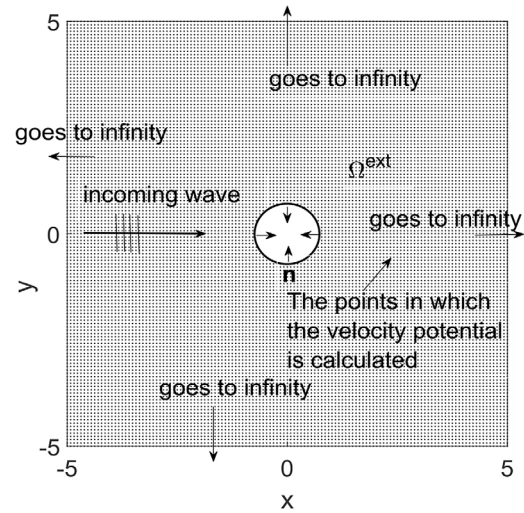


Figure 1. The external region under consideration is illuminated by plane, time-harmonic incident wave

boundary $\Gamma = I \cup S$ (Fig. 2). Due to the homogeneous Neumann boundary conditions, the third term of the Equation 7 vanishes. Now, the boundary integral Equation 7 for constant boundary elements can be written in terms of local coordinate ξ as follows:

$$c(r)\varphi(r) + \sum_{j=1}^M \varphi_j(r') \int_{-1}^{+1} \frac{\partial G(|r-r'|)}{\partial n} J(\xi) d\xi = \varphi^{inc}(r) \quad (8)$$

where: M – is the total number of constant elements, and $J(\xi)$ – is the Jacobian of transformation defined as:

$$J(\xi) = \frac{d\Gamma}{d\xi} = \sqrt{\left(\frac{dx(\xi)}{d\xi}\right)^2 + \left(\frac{dy(\xi)}{d\xi}\right)^2} = \frac{L}{2} \quad (9)$$

where: L is the length of the constant boundary element [30, 32–34].

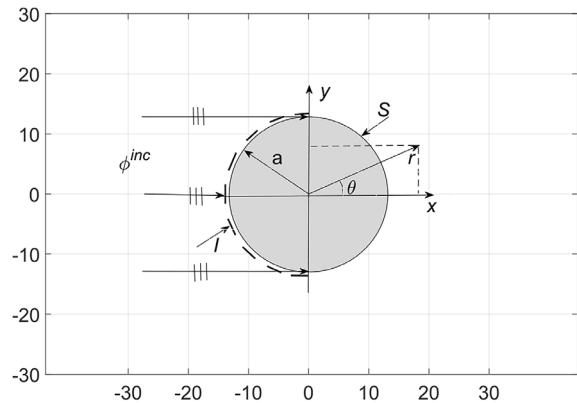


Figure 2. Circular scatterer illuminated by incident plane wave where I denote the illuminated and S represents the shadowed zone

If the incident plane wave is traveling along the vector $\mathbf{d}_j = (\cos \theta_j, \sin \theta_j)$ than $\varphi^{inc}(\mathbf{r}) = e^{i\mathbf{k}\mathbf{r} \cdot \mathbf{d}_j}$, where i is the imaginary unit $i = \sqrt{-1}$.

It is worth noticing that the unit vector is defined in the boundary element method by the x-component and y-component of the unit outward vector. So, the incident wave is easy to calculate on the boundary and incorporated into the right-hand side of the Equation 8. Equation 8 describes the acoustic forward scattering problem presented in Figure 1 and in Figure 2. The direct (forward) problem is used in the iterative solution of the inverse acoustic problem.

THE INVERSE PROBLEM OF ACOUSTIC SCATTERING

In order to calculate the inverse problem, it is necessary to define the state function $\varphi(\mathbf{p})$ (see Equation 3), objective function, and inequality constraints. Then, the boundary conditions and parameters of the acoustic environment must be established. The perturbed circular cross-section of the scatterer boundary is rigid. That is why the homogeneous Neumann boundary conditions on the obstacle were imposed. The external area is homogenous and is filled by the air. The velocity of the sound wave is equal to 344 [m/s] [27].

Definition of the objective function

The following objective function (Equation 10) has been defined to match the signal calculated in each iteration step to the measured one on the boundary. The analysis was conducted in the frequency domain, which means that all signals are complex and have real and imaginary parts.

This auxiliary function will be a part of the objective function and will be subject to depreciation with certain nonlinear constraints:

$$\hat{\Phi} = \sum_{j=1}^{j=p} \hat{\Phi}_j = \sum_{j=1}^{j=p} (f_j - \hat{v}_{0j}) = \sum_{j=1}^{j=p} \text{Re}(f_j - \hat{v}_{0j}) + j \sum_{j=1}^{j=p} \text{Im}(f_j - \hat{v}_{0j}) \quad (10)$$

where: $\hat{\Phi}$ means complex quantities, $\hat{\Phi}_j$ – global auxiliary complex function taken from p sensors calculated along boundary Γ (see Figure 3), $\hat{\Phi}_j$ – auxiliary complex function for the j – th sensor of the velocity potential difference between so called “measured” and calculated in each iteration step, f_j value representing the

calculated complex signal for the current iterative step, \hat{v}_{0j} – measured velocity potential for the j – th sensor on the Γ circle.

Now Equation 11 could be shown in the following compact form:

$$\hat{\Phi} = \sum_{j=1}^{j=p} \hat{\Phi}_j = \sum_{j=1}^{j=p} \text{Re} \hat{\Phi}_j + j \sum_{j=1}^{j=p} \text{Im} \hat{\Phi}_j \quad (11)$$

To minimize the objective function, it must be the real number, so must be defined by the following Equation 12:

$$F = \sum_{j=1}^{j=p} (\hat{\Phi}_j \hat{\Phi}_j^*) = \sum_{j=1}^{j=p} (\text{Re}^2 \hat{\Phi}_j + \text{Im}^2 \hat{\Phi}_j) \quad (12)$$

where: $\hat{\Phi}_j^*$ means complex conjugate to auxiliary function $\hat{\Phi}_j$.

From the physical point of view the objective function F is a distance in the complex plane between the measured and calculated signal. Minimization of a distance means that both signals become the same one or almost the same when the measured signal is polluted by the noise.

The definition of inequality constraints

The problem of acoustic imaging has been reduced to the issue of optimization, i.e., de facto to the search for the optimal shape of the edge of the object to be imaged. During the optimization process, the scatterer should be expressed in terms of the boundary Γ . Such demands mathematically could be express in the following way:

$$\begin{bmatrix} -1 & 0 & 0 & 0 \\ 1 & 0 & 0 & 0 \\ 0 & -1 & 0 & 0 \\ 0 & 1 & 0 & 0 \\ 0 & 0 & -1 & 0 \\ 0 & 0 & 1 & 0 \\ 0 & 0 & 0 & -1 \\ 0 & 0 & 0 & 1 \end{bmatrix} \begin{bmatrix} R \\ \varepsilon \\ mvx \\ mvy \end{bmatrix} < \text{radius of the} \begin{bmatrix} -0.5R_r \\ 0.8R_r \\ -0.001 \\ 1 \\ -0.01R_r \\ 0.6R_r \\ -0.01R_r \\ 0.6R_r \end{bmatrix} \quad (13)$$

where: R – radius of the perturbed circle of the scatterer, R_r – radius of the circle with the sensors, which is the constant value, ε – optimization variable responsible for the amplitude corrugation, mvx – x component of the position vector of the region to be imaged and mvy – y component of the position vector.

The crucial point of any Inverse Problems solved by the Optimization Approach is the Sensitivity Analysis, which is particularly difficult for BEM [28]. So, to avoid the Sensitivity Analysis, which is complicated and time-consuming for BEM, the `fmincon` function

was selected from the MATLAB library. This function calculates the gradient of the objective function numerically, so it is very convenient because the user does not need to deal with the Sensitivity Analysis at all. This function can effectively find the minimum of the constrained nonlinear multivariable objective function.

NUMERICAL EXAMPLES

Numerical examples have been presented to demonstrate the effectiveness of this approach and the dependence of the results on various parameters. The measurement data was taken at the boundary gamma in points where the acoustic sensors were placed (see Fig. 3). In this example, only eight sensors were located.

A nonconvex scatterer was considered a corrugated circle (see Fig. 3). A quite simple parametric Equation could describe the boundary of such a scatterer [27, 35]:

$$x = g \cos(\theta); y = g \sin(\theta) \quad (14)$$

where: the function g could be defined in a following way:

$$g = \varepsilon \lambda (a_v \sin(a_s \theta) + b_v \sin(b_s \theta)) + \lambda a_r \quad (15)$$

where: $\lambda, \varepsilon, a_v, a_s, b_v, b_s$ and a_r are the coefficients responsible for the shape of the scatterer.

Different coefficients of function g correspond to various shapes of scatterers [27, 35]:

- for the circle:

$$\lambda = 1; a_r = 1; \varepsilon = 0 \quad (16)$$

- for a kite:

$$a_v = 0.5; b_v = 0.8; \lambda = 1; a_r = 0; \varepsilon = 0 \quad (17)$$

- for a corrugated circle/cylinder:

$$a_v = 0.5; b_v = 0.5; a_s = 6; b_s = 7; \lambda = 1; a_r = 0; \varepsilon = 0.4 \quad (18)$$

The focus of this paper is on the corrugated circle. Using the parametric Equation 15, different shapes of the obstacle can be generated. Such parametric description might be particularly useful in the scattering exterior (see Fig. 1) inverse problems solved by BEM [26–28].

NUMERICAL EXPERIMENTS RESULTS

Four numerical experiments were carried out using MATLAB software to prove the efficiency of the proposed approach to the inverse scattering acoustic problem for the near field data. The first was conducted for the measurement height $h = 0.15 \lambda$, the amplitude of perturbation $\varepsilon = 0.02$, and noise level $\delta = 10\%$. In this case, the influence of the number of sensors on the optimization results was studied. Figure 4 shows the “measured” boundary function (solid line) and the

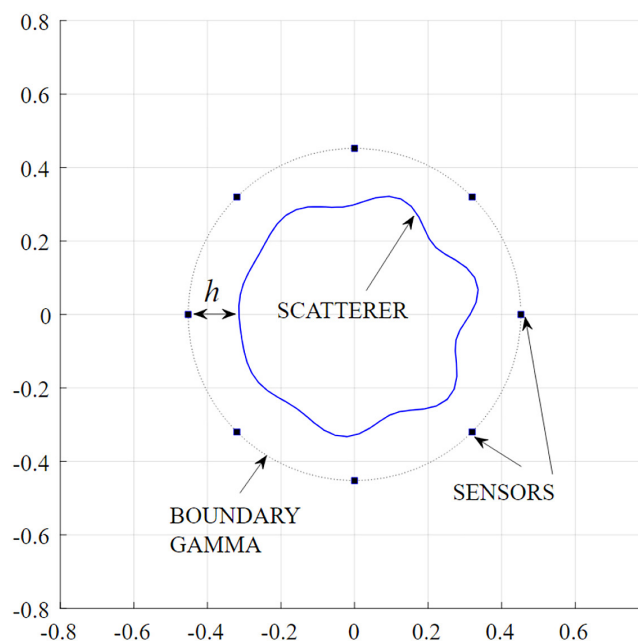


Figure 3. Circular corrugated scatterer illuminated by plane wave with eight sensors fixed in the boundary Γ

reconstructed boundary function (dashed line) for $n = 8$, $n = 16$ and $n = 32$, respectively. It is worth mentioning that the circle marked by the yellow color (without the perturbation) is the starting position for optimization. The dashed line indicates the optimization results, whereas the solid line means the real position and shape. This is obligatory for all subsequent figures. All numerical experiments for different parameters have been started from the same position. The delicate features of the obstacle are well reconstructed. However, the accuracy will not be significantly higher if the number of sensors increases, as shown in Figure 4.

For the next experiment, with fixed parameters height $h = 0.15 \lambda$ and noise level $\delta = 10\%$ the effects of the perturbation parameter ε were analyzed. Figure 5 shows the “measured” (solid line) and the reconstructed boundary function (dashed line) for $\varepsilon = 0.02$, 0.03 and 0.04 , respectively. Figure 5 shows the results even for relatively high 10% noise added to the measurements

for different amplitude of perturbations parameter ε are stable and precise.

In the third experiment, the effects of the noise level δ were investigated, maintaining constant parameters $\varepsilon = 0.04$ and $h = 0.15 \lambda$. Figure 6 shows the “measured” (solid line) and the reconstructed (dashed line) boundary function for $\delta = 1\%$, 10% and 20% , respectively. As expected, the reconstruction deteriorates as δ increases. As evident in Figure 6, the influence of the noise level is significant, which was expected; however, even at a 20% noise level, some helpful information can still be obtained.

The latest experiment analyzed the effect of the measurement distance h for $\varepsilon = 0.04$, $\delta = 5\%$. Figure 7 shows the exact (solid) and the reconstructed (dashed) boundary line for $h = 0.2 \lambda$, 0.1λ , and 0.05λ , respectively. Clearly, as distance h decreases, the precision of reconstruction increases. But increasing is not impressive. The most important thing is that the distant h must belong to the near-field data.

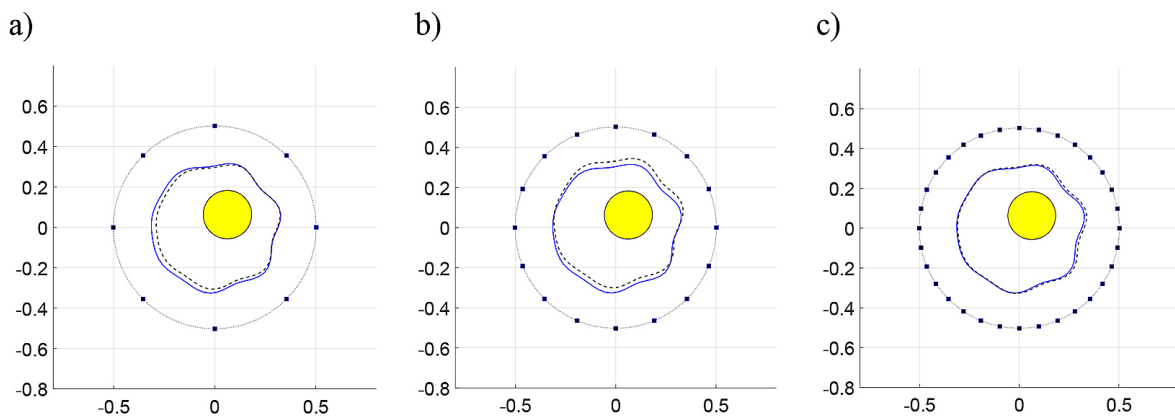


Figure 4. Effect of sensors number: “measured” shape (solid line) and reconstructed surface function (dashed line) for $\varepsilon = 0.02$, $h = 0.15 \lambda$, $\delta = 10\%$ and a) $n = 8$, b) $n = 16$, c) $n = 32$ sensors

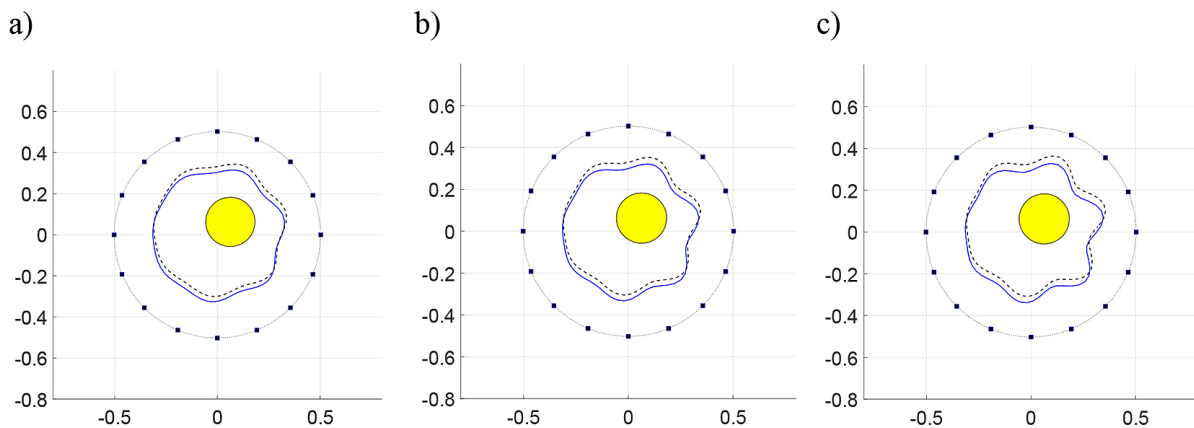


Figure 5. Exact (solid line) and reconstructed (dashed line) surface function for $h = 0.15 \lambda$. $\Delta = 10\%$, and $n = 16$: a) $\varepsilon = 0.02$, b) $\varepsilon = 0.03$, c) $\varepsilon = 0.04$

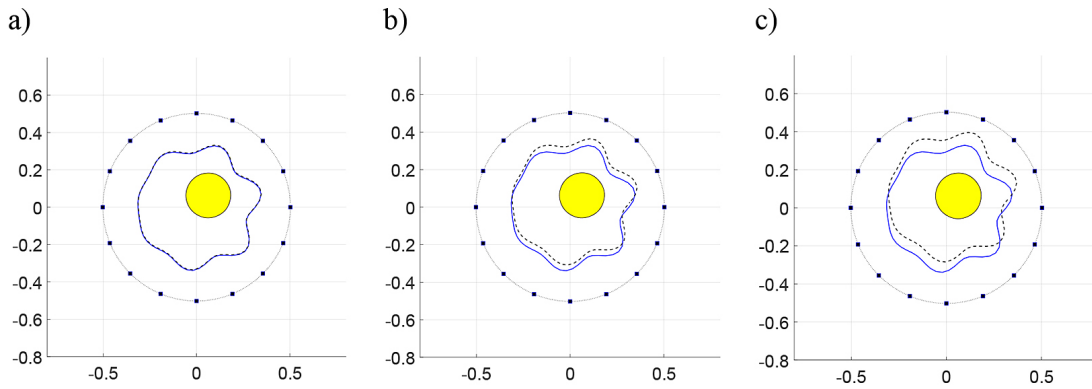


Figure 6. Effect of sensors number: “measured” boundary (solid line) and reconstructed (dashed line) surface function for $\epsilon = 0.04$, $h = 0.15\lambda$, $n=16$: a) $\delta = 1\%$, b) $\delta = 10\%$, c) $\delta = 20\%$

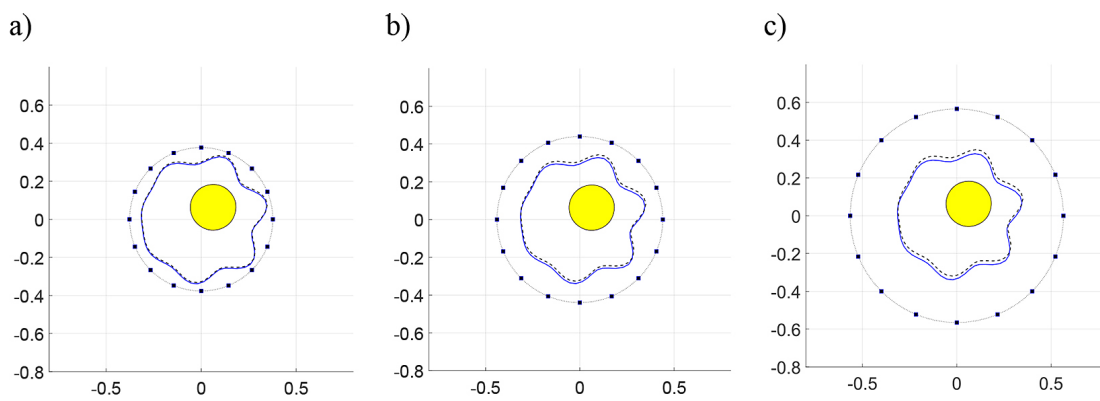


Figure 7. Sensor-to-object distance effect – h : “measured” shape (solid line) and reconstructed surface function (dashed line) for $\epsilon = 0.04$, $\delta = 5\%$, $n=16$: a) $h = 0.05 \lambda$, b) $h = 0.1 \lambda$, c) $h = 0.2 \lambda$

CONCLUSIONS

The Inverse acoustic scattering problem in 2D space for the near field data was presented in this paper. The classical BEM was used for the solution, and The Objective function, Boundary conditions, and inequality constraints were defined. Analyzing the acoustic problems is not easy for the classical BEM, but keeping the number of boundary elements per wavelength much more above the lower limit equal to 10, the error was kept low.

The main goal of this paper was to investigate if such an approach is suitable for imagining acoustic problems. Using BEM, we could concentrate only on the boundary. The boundary was parametrized to reduce the number of optimization parameters, allowing the achievement of arbitrary shapes. The results of controlling different parameters are shown in the figures. On this basis, it could be stated that the proposed approach produces reliable results when using near-field data

as well as very robust concerning the noise. Another important conclusion, from a practical point of view, is that the number of sensors does not have to be exceedingly high.

The presented method demonstrates a robust and reliable approach for solving inverse acoustic scattering problems using near-field data. It also highlights its practical applicability in various engineering fields by maintaining low error rates with an optimal number of sensors and handling noise effectively.

REFERENCES

1. Venås JV, Kvamsdal T. Isogeometric boundary element method for acoustic scattering by a submarine. *Comput Methods Appl Mech Eng* 2020; 359: 112670. <https://doi.org/10.1016/J.CMA.2019.112670>
2. Wu SW, Xiang Y. A coupled hybrid smoothed radial point interpolation method for computing underwater acoustic scattering.

- Physics of Fluids 2023; 35: 107103. <https://doi.org/10.1063/5.0167514/2914207>
3. Rymarczyk T, Sikora J. Some more on logarithmic singularity integration in boundary element method. *Informatyka, Automatyka, Pomiary w Gospodarce i Ochronie Srodowiska* 2024; 14: 5–10. <https://doi.org/10.35784/IAPGOS.5864>
 4. Chen L, Zhao J, Lian H, Yu B, Atroshchenko E, Li P. A BEM broadband topology optimization strategy based on Taylor expansion and SOAR method—Application to 2D acoustic scattering problems. *Int J Numer Methods Eng* 2023; 124: 5151–82. <https://doi.org/10.1002/NME.7345>
 5. Fakhraei J, Arcos R, Pàmies T, Romeu J. 2.5D singular boundary method for exterior acoustic radiation and scattering problems. *Eng Anal Bound Elem* 2022; 143: 293–304. <https://doi.org/10.1016/J.ENGANABOUND.2022.06.017>
 6. Wei Y, Wang B, Qian Z. A Modified Boundary Element Solution for Ultrasonic Guided Wave Mode-Conversion and Scattering in Curved Plates. *Proceedings of the 2022 16th Symposium on Piezoelectricity, Acoustic Waves, and Device Applications, SPAWDA 2022*; 2022: 567–71. <https://doi.org/10.1109/SPAWDA56268.2022.10045862>
 7. Yang F, Peng Z, Song H, Tang Y, Miao X. A hybrid finite element method – Kirchhoff approximation method for modeling acoustic scattering from an underwater vehicle model with Alberich coatings with periodic internal cavities. *Archives of Acoustics* 2024; 49: 209–219. <https://doi.org/10.24425/AOA.2024.148777>
 8. Ilnicki A, Rzasa MR. Numerical modelling of engine operation with a variable state of compression. *CEUR Workshop Proc* 2023; 3628: 282–92.
 9. Bilynsky Y, Nikolsky A, Revenok V, Pogorilyi V, Smailova S, Voloshina O, Kumargazhanova S. Convolutional neural networks for early computer diagnosis of child dysplasia. *Informatyka, Automatyka, Pomiary w Gospodarce i Ochronie Srodowiska* 2023; 13: 56–63. <https://doi.org/10.35784/IAPGOS.3499>
 10. Kłosowski G, Rymarczyk T, Niderla K, Kulisz M, Skowron Ł, Soleimani M. Using an LSTM network to monitor industrial reactors using electrical capacitance and impedance tomography – a hybrid approach. *Eksploatacja i Niezawodność* 2023; 25. <https://doi.org/10.17531/EIN.2023.1.11>
 11. Kozłowski E, Borucka A, Oleszczuk P, Jałowicz T. Evaluation of the maintenance system readiness using the semi-Markov model taking into account hidden factors. *Eksploatacja i Niezawodność* 2023; 25. <https://doi.org/10.17531/EIN/172857>
 12. Korzeniewska E, Zawisłak R, Szymon P, Bilaska A, Sarna P. Selection of wireless communication technology for data transmission between wearable electronics devices and the receiver. *Przeład Elektrotechniczny* 2023; 2023: 303–6. <https://doi.org/10.15199/48.2023.12.57>
 13. Schanz M. Realizations of the generalized adaptive cross approximation in an acoustic time domain boundary element method. *PAMM* 2023; 23: e202300024. <https://doi.org/10.1002/PAMM.202300024>
 14. Liu C, Hu G, Xiang J, Zhang J. Uniqueness to inverse acoustic and elastic medium scattering problems with hyper-singular source method 2024.
 15. Peake MJ, Trevelyan J, Coates G. Extended isogeometric boundary element method (XIBEM) for three-dimensional medium-wave acoustic scattering problems. *Comput Methods Appl Mech Eng* 2015; 284: 762–80. <https://doi.org/10.1016/J.CMA.2014.10.039>
 16. Wajman R, Nowakowski J, Łukiański M, Banasiak R. Machine learning for two-phase gas-liquid flow regime evaluation based on raw 3D ECT measurement data. *Bulletin of the Polish Academy of Sciences: Technical Sciences* 2024; 72. <https://doi.org/10.24425/BPASTS.2024.148842>
 17. Wajman R. The concept of 3D ECT system with increased border area sensitivity for crystallization processes diagnosis. *Sensor Review* 2021; 41: 35–45. <https://doi.org/10.1108/SR-10-2019-0254>
 18. Charalambopoulos A, Gergidis L, Vassilopoulou E. A conditioned probabilistic method for the solution of the inverse acoustic scattering problem. *Mathematics* 2022; 10: 1383. <https://doi.org/10.3390/MATH10091383>
 19. Heronimczak M, Mrowiec A, Rząsa M, Koszela K. Measurements of the flow of a liquid–solid mixture/suspension through a segmented orifice. *Sci Rep* 2024; 14. <https://doi.org/10.1038/S41598-023-50737-6>
 20. Poblet-Puig J, Rodríguez-Ferran A. The finite strip method for acoustic and vibroacoustic problems. <https://doi.org/10.1142/S0218396X11004456> 2012; 19: 353–78. <https://doi.org/10.1142/S0218396X11004456>
 21. Albin N. High-order numerical methods for nonlinear acoustics: A Fourier Continuation approach. *J Acoust Soc Am* 2012; 132: 1919–1919. <https://doi.org/10.1121/1.4755041>
 22. Becker AA. *The boundary element method in engineering : a complete course*. McGraw-Hill; 1992.
 23. Colton D, Kress R. *Integral equation methods in scattering theory*. Springer; 1993.
 24. Baynes AB. *Scattering of low-frequency sound by compact objects in underwater waveguides*. PhD Dissertation. Naval Postgraduate School, 2018.
 25. Jeong C, Na SW, Kallivokas LF. Near-surface localization and shape identification of a scatterer

- embedded in a halfplane using scalar waves. *Journal of Computational Acoustics* 2011; 17: 277–308. <https://doi.org/10.1142/S0218396X09003963>
26. Li P, Wang Y. Numerical solution of an inverse obstacle scattering problem with near-field data. *J Comput Phys* 2015; 290: 157–68. <https://doi.org/10.1016/J.JCP.2015.03.004>
27. Kirkup S. The boundary element method in acoustics: a survey. *Applied Sciences* 2019; 9: 1642. <https://doi.org/10.3390/APP9081642>
28. Kirkup S. The boundary element method in acoustics. A development in Fortran; 2007.
29. Sikora J. Forward acoustic problem analyzed by boundary element method. *Przegląd Elektrotechniczny* 2023; 99: 274–7. <https://doi.org/10.15199/48.2023.01.55>
30. Jabłoński P. Engineering Physics–Electromagnetism. Częstochowa University of Technology; 2009.
31. I-Campus: Waves Module n.d. <http://web.mit.edu/fluids-modules/waves/www/c-index.html> (accessed July 2, 2024).
32. Rymarczyk T. Tomographic imaging in environmental, industrial and medical applications. Innovation Press Publishing Hause; 2019.
33. Abramowitz M, Stegun IA. Handbook of mathematical functions with formulas, graphs, and mathematical tables. New York: John Wiley; 1973.
34. Sikora J. Boundary element method for impedance and optical tomography. Warsaw University of Technology Publishing Hause; 2007.
35. Lynott GM. Efficient numerical evaluation of the scattering of acoustic and elastic waves by arrays of cylinders of arbitrary cross section. PhD Dissertation. University of Manchester, 2020.